

Mining Limited Data Sufficiently: A BERT-inspired Approach for CSI Time Series Application in Wireless Communication and Sensing

Zijian Zhao, Fanyi Meng, Hang Li, Xiaoyang Li, Guangxu Zhu

Abstract—Channel State Information (CSI) is the cornerstone in both wireless communication and sensing systems. In wireless communication systems, CSI provides essential insights into channel conditions, enabling system optimizations like channel compensation and dynamic resource allocation. However, the high computational complexity of CSI estimation algorithms necessitates the development of fast deep learning methods for CSI prediction. In wireless sensing systems, CSI can be leveraged to infer environmental changes, facilitating various functions, including gesture recognition and people identification. Deep learning methods have demonstrated significant advantages over model-based approaches in these fine-grained CSI classification tasks, particularly when classes vary across different scenarios. However, a major challenge in training deep learning networks for wireless systems is the limited availability of data, further complicated by the diverse formats of many public datasets, which hinder integration. Additionally, collecting CSI data can be resource-intensive, requiring considerable time and manpower.

To address these challenges, we propose CSI-BERT2 for CSI prediction and classification tasks, effectively utilizing limited data through a pre-training and fine-tuning approach. Building on CSI-BERT1, we enhance the model architecture by introducing an Adaptive Re-Weighting Layer (ARL) and a Multi-Layer Perceptron (MLP) to better capture sub-carrier and timestamp information, effectively addressing the permutation-invariance problem. Furthermore, we propose a Mask Prediction Model (MPM) fine-tuning method to improve the model's adaptability for CSI prediction tasks. Experimental results demonstrate that CSI-BERT2 achieves state-of-the-art performance across all tasks with relatively fast computation speeds. To facilitate future research, we will make our code and dataset publicly available upon publication.

Index Terms—Channel State Information (CSI), CSI Prediction, CSI Classification, Wireless Communication, Wireless Sensing

I. INTRODUCTION

Channel State Information (CSI) plays a critical role in both wireless sensing and wireless communication systems by capturing the propagation characteristics of the wireless channel. This information provides valuable insights into the

radio environment, including the channel conditions, signal quality, and the motion and location of objects. In wireless communication systems, CSI is essential for optimizing various processes such as channel compensation, adaptive modulation and coding, user selection and scheduling. By effectively utilizing CSI, these systems can achieve better performance, increased spectrum efficiency, and more reliable communication, ultimately enhancing the overall user experience [1]–[3]. In wireless sensing applications, CSI can enhance the ability to detect and track objects, leading to improved environmental awareness. With the advantage of privacy protection, low cost, and penetration ability, wireless sensing has been widely used in many areas like fall detection [4], localization [5], and people identification [6].

Despite the importance of CSI in wireless systems, it is challenging to acquire, process, and utilize CSI data. For example, many deep learning methods in wireless systems require substantial data for training, but the data available in wireless communication is often limited, and public datasets may have different formats, making it challenging to use them together [6]. Additionally, collecting CSI datasets on one's own can be a difficult task.

A common solution for data scarcity is pre-training, which has been widely utilized in fields such as Natural Language Processing (NLP) [7], [8], Computer Vision (CV) [9], [10], and Music Information Retrieval (MIR) [11], [12]. The pre-training process typically employs a self-supervised approach, enabling models to learn the underlying structure and patterns of the data. This can enhance the model's performance on downstream tasks, as well as improve its convergence speed and generalization capacity, particularly in scenarios with limited training data [13], [14]. Pre-training not only allows models to learn and understand the data more effectively, but it also enables the use of additional unlabeled data for training. Currently, pre-training is not exclusively applied to address data scarcity. In fields such as NLP and CV, as datasets continue to grow, pre-training has emerged as a powerful strategy to bolster model generalization capacity [15], [16]. Moreover, even when the inference scenario differs from the training scenario, models can quickly adapt to new contexts through transfer learning methods [17], [18], such as fine-tuning.

Even though, pre-training and fine-tuning models on different datasets is uncommon in certain specialized fields, such as MIR and signal processing, which often face challenges due to limited data. On one hand, some tasks lack additional data

Part of the work was presented in 2024 IEEE International Conference on Computer Communications (INFOCOM) DeepWireless Workshop.

* Corresponding Author: Guangxu Zhu

Zijian Zhao is with Shenzhen Research Institute of Big Data, Shenzhen 518115, China, and also with the School of Computer Science and Engineering, Sun Yat-sen University, Guangzhou 510275, China (e-mail: zhaozj28@mail2.sysu.edu.cn)

Fanyi Meng, Hang Li, Xiaoyang Li, and Guangxu Zhu are with the Shenzhen Research Institute of Big Data, The Chinese University of Hong Kong (Shenzhen), Shenzhen 518115, China (e-mail: fanyimeng@link.cuhk.edu.cn; hangdavidli@sribd.cn; lixiaoyang@sribd.cn; gxzhu@sribd.cn)

for pre-training. On the other hand, simply fine-tuning a pre-trained model on a new dataset may result in poor performance when the pre-training data is insufficient. Consequently, most research in these fields opts to pre-train and fine-tune models using the same dataset [19]. The unsupervised learning during the pre-training phase effectively helps models extract valuable insights from the limited data available.

Bidirectional Encoder Representations from Transformers (BERT) [20] is a pioneering work that first explored the efficiency of pre-training method in NLP. With the help of its bi-directional attention mechanism, which efficiently extracts the relationship of context, and the Mask Language Model (MLM) pre-training task, which helps the model learn the basic data structure, BERT has become the foundation for current understanding models. Since wireless information sequences also exhibit contextual relationships like natural language, BERT can also be used to extract their inherent features. Previous researchers have explored the application of BERT in wireless sensing tasks, including localization [21], [22] and radio maps construction [23]. However, most of these studies directly convert continuous wireless signals into discrete tokens, resulting in significant information loss. Additionally, their approach simply adapted BERT from NLP without any customized design, which is not suitable due to the different structure of wireless signals and natural language.

In contrast, we have previously proposed a model named CSI-BERT1 [24] for CSI recovery. By redesigning the structure of BERT, we make it more suitable for CSI sequences, such as using a linear layer-based token embedding to replace the traditional tokenization method and designing a time embedding for CSI time series. While CSI-BERT1 has shown promising performance, we have identified some shortcomings, such as the permutation invariance of the time embedding [25] and the gap between training and inference.

In this paper, we address these issues by optimizing both the model structure and the training process, as illustrated in Fig. 1. We further introduce CSI-BERT2 for CSI prediction and classification. By incorporating a novel embedding layer that effectively captures the relationships between subcarriers and timestamps, our model demonstrates a robust capability for processing CSI time series. Additionally, by designing and utilizing the [MASK] token within the CSI series, we enable our model to adapt to various wireless scenarios, as shown in Fig. 2. We evaluate our model on two publicly available datasets, WiGesture [24] and WiFall [26], along with a self-collected dataset, WiCount. The experimental results indicate that CSI-BERT2 achieves state-of-the-art performance across all tasks. In summary, the main contributions of this work are:

(1) A Multifunctional Framework for CSI Time Series:

We propose CSI-BERT2, a multifunctional model for CSI time series applications in wireless systems, including CSI prediction and CSI classification. To realize these, we optimize the structure and training process of the original CSI-BERT1 model.

(2) Improved Model Structure:

We design a novel time embedding technique that using Multi-Layer Perceptron (MLP) to further encode time information, to solve the permutation invariant problem of the encoder structure, which can be

detrimental for time series. Second, we use a simple attention mechanism called Adaptive Re-Weighting Layer (ARL) to better capture the relationships between subcarriers.

(3) Improved Training Process: To make full use of the limited data, we first pre-train the model in a unsupervised manner by MLM task and then fine-tune it in specific downstream tasks. Specifically, we propose a Mask Prediction Model (MPM) fine-tune method to make the encoder structure more suitable for prediction tasks.

(4) Experiment Evaluation: Experimental results demonstrate that our CSI-BERT2 model outperforms all other models across all tasks. In the CSI prediction task, it achieves the lowest error while maintaining relatively fast computation speeds. In the CSI classification task, it attains the highest accuracy in various applications, including gesture recognition, people identification, fall detection, and crowd counting. Notably, it can directly utilize discontinuous data caused by packet loss and effectively handle scenarios where the testing set has a different sampling rate than the training set, even when the training set itself has varying sampling rates.

The structure of this paper is organized as follows. In Section II, we first introduce the fundamental principles of CSI, along with the background on CSI prediction and classification. We also review relevant works in these areas. In Section III, we provide a detailed description of the model structure and the training process for different tasks. In Section IV, we present a series of comparative experiments to demonstrate the advantages of our method, along with several ablation studies to illustrate the efficiency of our design. Finally, in Section V, we summarize the paper and highlight potential directions for future research.

II. PRELIMINARY

A. CSI Basics

Following [27], in Wi-Fi communication, CSI characterizes the way Wi-Fi signals propagate from the transmitter (TX) to the receiver (RX). The amplitude and phase of CSI are influenced by multipath effects, which include amplitude attenuation and phase shift. Each element of the CSI Matrix H can be given by:

$$H(f; t) = \sum_{n=1}^N a_n(t) e^{-j2\pi f \tau_n(t)}, \quad (1)$$

where N is the number of paths between the TX and the RX, $a_n(t)$ is the amplitude attenuation factor, $\tau_n(t)$ is the propagation delay, f is the carrier frequency, and t is the timestamp.

B. CSI Prediction

In wireless communication, obtaining the CSI matrix is a challenging task, especially in future mmWave scenarios [28]. Considering the large number of antennas, the dimension of the CSI matrix will also be substantial, significantly increasing the complexity of the channel estimation algorithms. On the other hand, when objects in the environment are moving at high speeds, the channel coherence time will be greatly

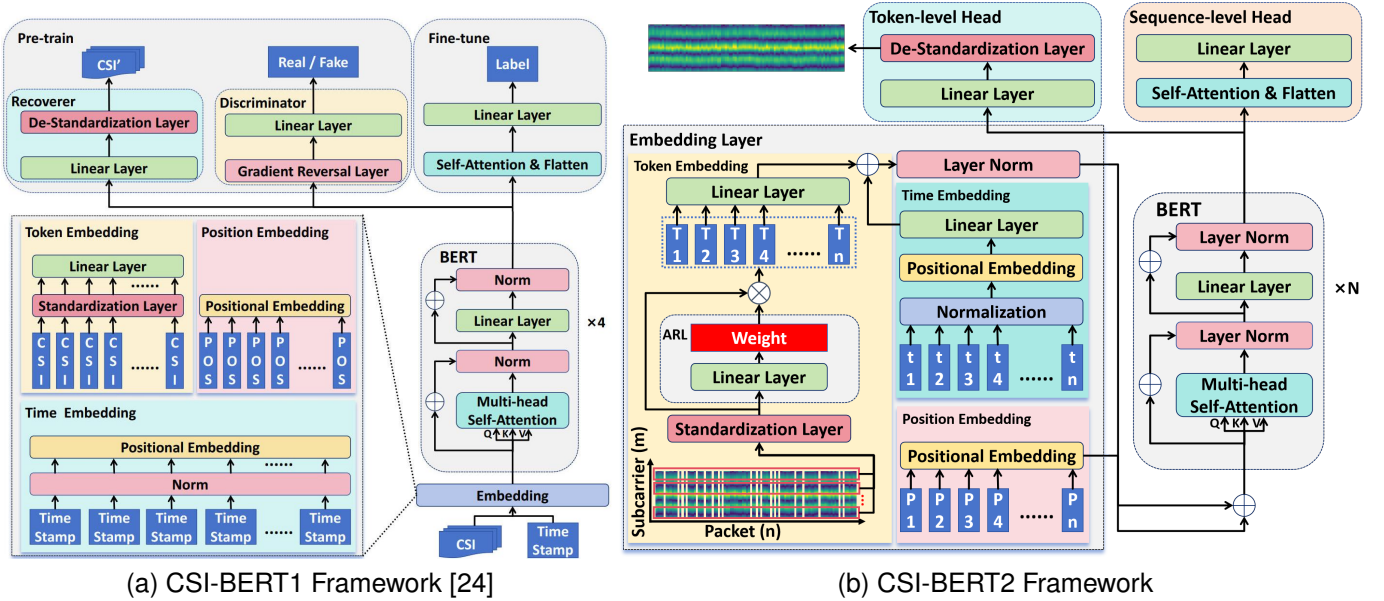


Fig. 1. Architecture of Two Generations of CSI-BERT: In Fig. 1b, ‘T’ represents token, ‘t’ represents time stamp, and ‘P’ represents the position.

reduced, thereby increasing the requirements for channel estimation time. Nevertheless, shown as Fig. 2a, CSI is crucial for optimizing wireless communication systems, making rapid estimation essential. Moreover, if we can predict future CSI in advance, we will have more time available for system optimizations, such as channel compensation.

Recently, some works have explored the use of additional information to predict CSI. In [29], the authors used multimodal sensory data, including received pilots, user’s position, and previous downlink CSI to predict the current CSI. In [30], a deep learning-based framework using a 3-D CNN architecture effectively predicts downlink channel state information by learning temporal, spatial, and frequency correlations from past channel sequences. [31] proposed an ML-based architecture for estimating channels by using CNN-AR, which achieves gains in prediction quality.

C. CSI Classification

In wireless sensing, many tasks can be framed as CSI classification, including gesture recognition [32], fall detection [4], and activity recognition [33]. Reviewing CSI basics, human movement in the environment can cause changes in the multi-path channel, which in turn changes the extracted CSI matrix. Therefore, by analyzing the pattern of changes in CSI, it is possible to sense human activities.

In real-world sensing systems, accurately characterizing human actions proves to be challenging. Complex actions, such as falling, kicking, and squatting, are particularly difficult to model mathematically. Additionally, noise in Wi-Fi extraction devices, including carrier frequency offset and sampling time offset, is hard to completely eliminate. These two challenges motivate the use of deep learning techniques for Wi-Fi sensing. In [34], the authors estimate human poses from videos to supervise the training of Wi-Fi CSI. The broad learning

system proposed in [35] aims to achieve fast and accurate Wi-Fi fingerprint localization. Furthermore, [36] introduces Wi-Mesh, a system that utilizes Wi-Fi signals and 2D angle-of-arrival (AoA) estimation to create 3D human meshes using deep learning, demonstrating effectiveness across various environments and conditions.

However, due to the instability of actual network environments, the receiver may struggle to successfully demodulate received signals due to several factors, including weak signal strength, frequency interference, and hardware errors. Moreover, packet loss itself may contain valuable sensing information. For instance, when an object obstructs the line-of-sight (LOS) path, the signal strength at the receiver (RX) significantly decreases, leading to an increase in packet loss. The discontinuous CSI resulting from packet loss can severely degrade the performance of wireless sensing models. Unfortunately, this issue has not been widely addressed in existing literature. Most studies attempt to use linear interpolation when the packet loss rate is low [37]. However, when the packet loss rate significantly increases, traditional interpolation fails to accurately reconstruct the true CSI, resulting in biased parameter estimation and incorrect inference.

To tackle this challenge, our previous work introduced CSI-BERT1 [24], a self-supervised learning method designed to capture the relationships within CSI data and recover lost packets. The recovered CSI can significantly enhance the capacity of sensing models. In this work, we further optimize the structure of CSI-BERT1 to improve its ability to capture temporal information, enabling it to successfully perform CSI classification tasks using the discontinuous CSI for training. Experimental results indicate that CSI-BERT2 achieves state-of-the-art performance in CSI classification tasks, greatly surpassing both CSI-BERT1 and other existing models. Consequently, there is no need to recover CSI separately for training other models. Moreover, with the aid of our proposed time

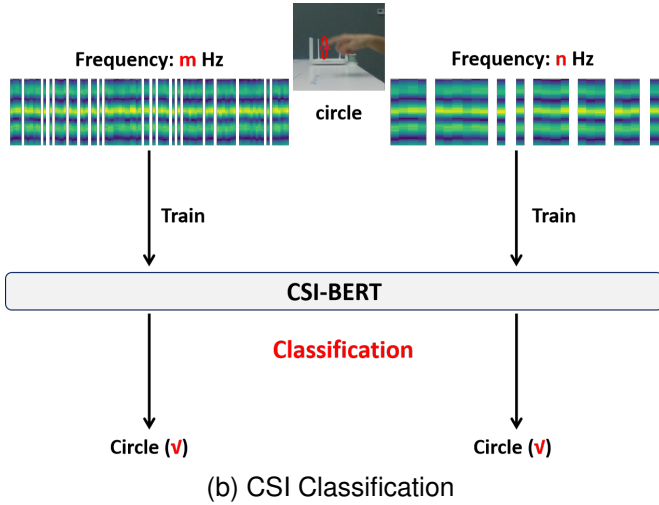
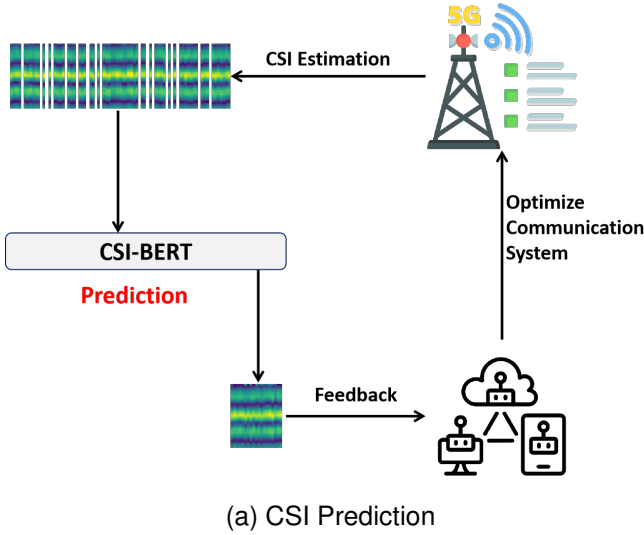


Fig. 2. Two Tasks in This Paper: (a) The CSI prediction task focuses on swiftly predicting future CSI series for proactive communication optimization. (b) The CSI classification task utilizes CSI for specific sensing applications, such as gesture recognition. Notably, our CSI-BERT2 can efficiently process CSI data at varying sampling rates, a challenge for most other models.

embedding layer, CSI-BERT2 can effectively handle scenarios where the testing set and training set have different sampling rates.

III. METHODOLOGY

A. Overview

The proposed CSI-BERT2 model is a BERT-based approach designed for CSI prediction, and classification, as illustrated in Fig. 1. The workflow of our model includes three phases: pre-training, fine-tuning, and inferring, as shown in Fig. 3. During pre-training, the CSI sequence is randomly destructured, and the model is trained to recover the missing components in a self-supervised manner, to make the model learn the CSI pattern and inner relationship. After that, the model can be fine-tuned for prediction tasks or classification tasks. Finally, the trained model can be used to infer for specific downstream tasks.

In this section, we leverage the CSI sequence $c = [c_1, c_2, \dots, c_n]$ and the corresponding timestamps $t =$

$[t_1, t_2, \dots, t_n]$ as input. Each c_i represents a flattened vector of the CSI matrix at time t_i , which contains the amplitude and phase information of subcarriers.

B. Data Process

Due to package loss, the received CSI series are always incomplete. Before inputting it to our model, we need to first identify where the package loss happens and use a placeholder [PAD] to occupy the place of lost packages. We judge whether package loss happens according to the gap between two successive timestamps. Given a sampling rate f , the ideal time gap between two successive timestamps should be $\Delta t = \frac{1}{f}$ seconds. Assume we receive a CSI series $[c_1, c_2, \dots, c_m]$ with corresponding timestamps $[t_1, t_2, \dots, t_m]$ with the unit of seconds. Then we can identify whether there is package loss and how many packages were lost between c_i and c_{i+1} . We calculate the lost package amount according to:

$$k = \text{round} \left(\frac{t_{i+1} - t_i}{\Delta t} \right), \quad (2)$$

Then we will add k [PAD] tokens between c_i and c_{i+1} . Besides, we also need to add k corresponding timestamps between t_i and t_{i+1} . We define the j^{th} added timestamp between t_i and t_{i+1} as:

$$t_{i,j} = t_i + \frac{t_{i+1} - t_i}{k} j + \epsilon_j, \quad (3)$$

where ϵ_j is a small noise. Our method to identify package loss is reasonable because after adding the [PAD] tokens, we found the package amount is very close to the theoretical amount when there is no package loss in our dataset.

C. Model Structure

The model structure of two generations of CSI-BERT is shown in Fig. 1. We utilize BERT [20] (the encoder part of a Transformer model [38]) as the backbone, but replace the bottom embedding layer and the top heads to adapt our data format and tasks.

1) *Embedding Layer*: Compared to CSI-BERT1 [24], the main change is in the embedding layer. Our model's embedding layer consists of three parts: token embedding, time embedding, and position embedding.

In the token embedding, we first use a standardization layer along the time dimension, as shown in Eq. 4:

$$\begin{aligned} \mu^{(j)} &= \frac{\sum_{i=1}^n c_i^{(j)}}{n}, \\ \sigma^{(j)} &= \sqrt{\frac{\sum_{i=1}^n (c_i^{(j)} - \mu^{(j)})^2}{n}}, \\ \text{Standard}(c_i^{(j)}) &= \frac{c_i^{(j)} - \mu^{(j)}}{\sigma^{(j)}}, \end{aligned} \quad (4)$$

where $c_i^{(j)}$ represents the j^{th} dimension of c_i , μ and σ represent the mean and standard deviation, respectively. We noticed that the distribution of CSI in each subcarrier changes significantly over time, so the standardization operation can help the model learn features better and mitigate the covariate

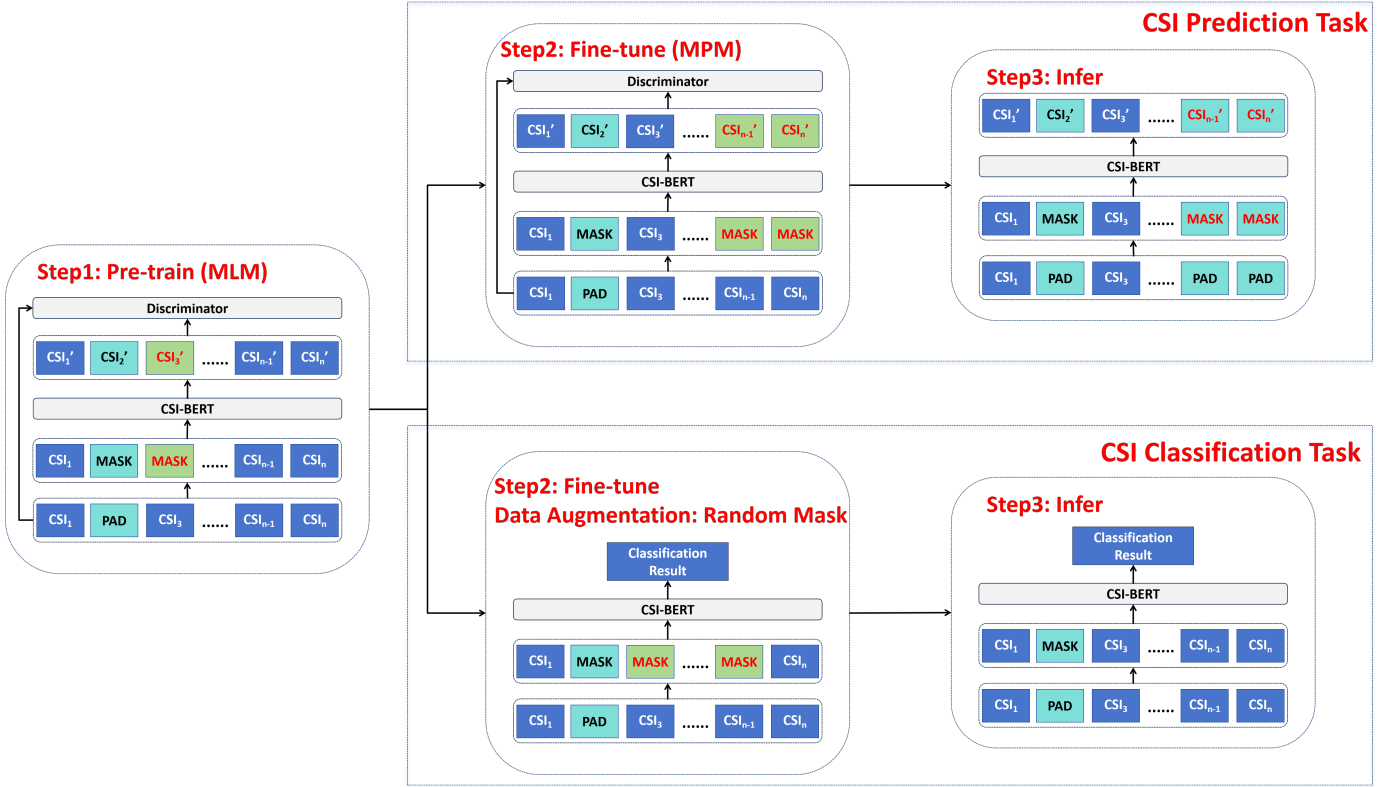


Fig. 3. Workflow: Similar to most pre-trained models, CSI-BERT2 also has three phases: pre-training, fine-tuning, and inference. In the figure, the [MASK] tokens with green background represent randomly added [MASK] tokens, the [MASK] tokens with blue background represent [MASK] tokens used to replace [PAD], the [MASK] tokens with red text represent the [MASK] tokens that the model is expected to recover or predict accurately, and the [MASK] tokens with black text represent [MASK] tokens whose corresponding outputs are not of concern.

shift problem [26], [39]. We also find it more efficient in CSI than other normalization operation like Batch Norm or Layer Norm.

Then, different from CSI-BERT1, we add an Adaptive Re-Weighting Layer (ARL) [40] along the subcarrier dimension to better capture the inner relationships, as shown in Eq. 5:

$$T = \text{MLP}(c) \cdot c, \quad (5)$$

where c is input, T is output token, and MLP represents a Multilayer Perceptron. ARL is a mechanism similar to attention but simpler and more efficient. It first uses an MLP to generate a weight vector and then multiplies it with the original input. This process ensures that the network assigns higher significance to subcarriers with more informative content and ignores those without much variation, such as guard carriers. Thereby, it can help enhance the model's precision and effectiveness. After that, another MLP will be used in the dimension of subcarrier to extract feature further.

For the time embedding layer, which accounts for the varying time intervals between consecutive CSI samples, we adopt a similar strategy as CSI-BERT1 but with an extra MLP to further embed the timestamp, as shown in Eq. 6:

$$\text{TE}(t_i)^{(j)} = \text{MLP} \left(\begin{cases} \sin\left(\frac{\text{Norm}(t_i)}{10^{\frac{4j}{d}}}\right), & j = 2k \\ \cos\left(\frac{\text{Norm}(t_i)}{10^{\frac{4(j-1)}{d}}}\right), & j = 2k + 1 \end{cases} \right), \quad (6)$$

$$\text{Norm}(t_i) = \frac{t_i - \min(t)}{\max(t) - \min(t)} L,$$

where j represents the j^{th} dimension of $\text{TE}(t_i)$, k is a positive integer, L is the maximum length of CSI sequence, and d is the dimension of each CSI vector c_i . We first normalize the timestamp and then use the positional embedding method to encode it. However, due to the permutation-invariant nature of the Transformer architecture, it can only capture distance information but not order information. Studies [25] have also shown that Transformer-based models do not perform very well on time series data. To solve this problem, we use an MLP to capture time information further. Then, the time embedding is added to the token embedding and fused together using Layer Normalization.

Finally, the position embedding layer is the same as in the traditional Transformer model, and the position embedding result is added to the fusion of token embedding and time embedding. It is used to represent the relative position, while the time embedding is used to represent the absolute position.

2) *Head Layer*: Similar to most BERT-based models, our CSI-BERT also has two branches for different tasks. The token-level head is used for CSI recovery and prediction tasks, while the sequence-level head is used for CSI classification tasks.

For the token-level head, a de-standardization layer is used to ensure that the output has a similar distribution as the input, as shown in Eq. 7:

$$\text{De-Standard}(y_i^{(j)}) = (y_i^{(j)} + \mu^{(j)}) * \sigma^{(j)}, \quad (7)$$

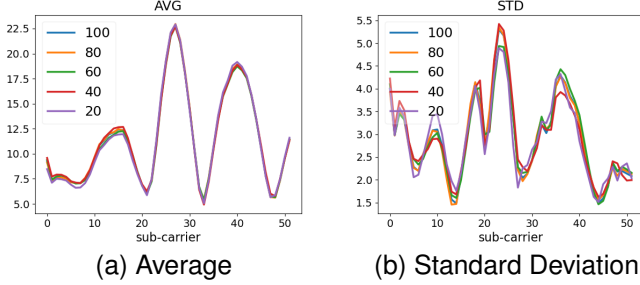


Fig. 4. Average and Standard Deviation of CSI Amplitude (WiGesture Dataset) [24]: Each line represents a different number of packets sampled from one second. The x-axis represents the subcarriers.

where y represents the output of the last linear layer, μ and σ are calculated using Eq. 4. We consider the de-standardization layer to be necessary and efficient. First, because the distribution information is discarded by the standardization layer, we can only provide this information by the de-standardization layer. Then, we notice that the mean and standard deviation of CSI are relatively stable within a small time window. For example, in Fig. 4, we use the WiGesture dataset [?] to illustrate the average and standard deviation of CSI amplitude for each subcarrier in one second. We randomly select some packets from a total of 100 packets and show their average and standard deviation, corresponding to each line. The result shows that even with a change in the number of packets, the two statistics do not change significantly. It also means that within different packet loss rates, the two statistics in one second would not have a large difference. As a result, we consider the de-standardization operation can help the model obtain a relatively realistic distribution information no matter in recovery task or prediction task.

For the sequence-level head, we use the same architecture as most Transformer-based methods [19], which first incorporates a self-attention layer to combine the features in the time dimension and then uses a linear layer to generate the final output.

D. Pre-training Phase

In the pre-training phase of CSI-BERT, we employ a similar approach to the MLM task in BERT [20]. This involves filling the empty positions with [PAD] tokens, randomly masking tokens with [MASK] tokens, and training the model to recover the masked tokens. However, due to the differences between continuous CSI and discrete natural language, we have made some modifications to adapt to the CSI data.

In BERT, the [MASK] token is a fixed token, but in CSI-BERT, we replace the word embedding layer with a linear layer, which means the [MASK] token can have different values affecting the output. To address this, we assign a random value to the [MASK] token, sampled from a Gaussian distribution as shown in Eq. 8 whose mean and standard deviation are calculated from the standardization layer. This random approach makes it more challenging for the model to identify the position of the [MASK] token, thereby improving

its understanding of the CSI sequence structure. Unlike CSI-BERT1, for the [PAD] token, even though we use a fixed value as [PAD], we replace it with [MASK] before inputting the CSI sequence to the model. This is because there is no [PAD] in the CSI recovery phase. Even though the [PAD] can be ignored by the attention mechanism through the attention mask matrix, it still affects the output of the ARL, which works in the dimension of subcarrier. If the [PAD] token only appears in the pre-training phase, it would cause a gap between inference and training, thereby influencing the model’s performance. As a result, we also cancel the attention matrix mechanism in this phase.

$$[MASK]_i^{(j)} \sim \mathcal{N}(\mu^{(j)}, \sigma^{(j)}), \quad (8)$$

For the pre-training phase, we follow a similar setting as RoBERTa [41] where some non-[PAD] tokens are randomly replaced with the [MASK] token. In RoBERTa, the masking proportion is fixed at 15%. However, in practical scenarios, the loss rate of CSI can vary, so we introduce a random masking proportion ranging from 15% to 70%, which is varied in each epoch.

Next, we train the model to recover these [MASK] tokens, where we refer to the model as the recoverer. To make the recovered CSI more realistic, we use an extra discriminator model. In CSI-BERT2, we use a GAN-based adversarial training strategy instead of the Domain Adversarial Neural Network (DANN) [42] based method in CSI-BERT1. While the DANN-based method has lower computational cost and faster training speed, the hyperparameter like gradient reversal rate λ in it is not easy to set, which is always dynamic during training. We found the same λ may not work when the training data changes, which may also cause the model to diverge. As a result, we select the Generative Adversarial Network (GAN) [43] based method in CSI-BERT2, where the discriminator does not share any parameters with the recoverer but has the same model structure. The optimization target of the GAN process can be represented as Eq. 9:

$$\begin{aligned} & \min_R \max_D V(D, R) \\ & = \min_R \max_D E_c[\log(D(c))] + E_c[\log(1 - D(R(c)))] , \end{aligned} \quad (9)$$

where D and R represent the discriminator and recoverer, respectively, and c represents the original CSI input. The discriminator tries to identify the original CSI input and the recovered CSI sequence output by the recoverer. Conversely, the recoverer tries to make it as confusing as possible, to make the recovered CSI more likely to be a real CSI sequence.

Specifically, the loss function of the recoverer consists of four parts, as shown in Eq. 10:

$$\begin{aligned} L_1 &= \text{MSE}(c, \hat{c}) , \\ L_2 &= \text{MSE}(\mu, \hat{\mu}) , \\ L_3 &= \text{MSE}(\sigma, \hat{\sigma}) , \\ L_4 &= \text{CrossEntropy}(D(\hat{c}), 1) , \end{aligned} \quad (10)$$

where \hat{c} represents the output of the recoverer, and $\hat{\mu}$ and $\hat{\sigma}$ represent the mean and standard deviation of \hat{c} in the time

dimension, respectively. The L_1 loss is the traditional loss function used in BERT, as it measures the accuracy of the output. However, in CSI recovery, the overall shape of the CSI is also important. Therefore, we utilize the L_2 and L_3 losses to consider the overall shape of the CSI by assessing its mean and standard deviation. Furthermore, the L_4 is the GAN loss for the recoverer, which tries to make the discriminator mistake in classifying the recovered CSI. Additionally, we calculate all the loss functions focusing only on the [MASK] tokens again to ensure that the model prioritizes the recovery of the missing CSI. What’s more, the loss function of the discriminator can be represented as Eq. 11:

$$L_{dis} = \text{CrossEntropy}(D(\hat{c}), 0) + \text{CrossEntropy}(D(c), 1), \quad (11)$$

Besides, unlike CSI-BERT1 that divides the CSI by a sliding window before training, we randomly select a CSI sequence from the whole dataset during training. This is an approach to mitigate the risk of over-fitting, as the fixed data division may make the model dependent on the absolute position. However, the absolute position actually only depends on the data division.

E. Fine-tuning Phase

1) *CSI Prediction Task*: Encoder-based methods like BERT [20] are often considered not suitable enough for generation or prediction tasks due to their bi-directional attention mechanisms. This is also influenced by their pre-training task, where MLM is used to train the model to recover the inner data, not the future data. However, decoder-based methods like GPT [8] and encoder-decoder based methods like BART [7] also suffer from the problem of error accumulation [25]. Since they generate data in an autoregressive manner, an error may also influence the further generation results. In contrast, encoder-based methods have the advantage that they can generate all data in one step.

To make CSI-BERT2 more suitable for the prediction task, we design a Mask Prediction Model (MPM). MPM has a similar format as MLM, but it only masks tokens at the end of the sequence instead of masking tokens in arbitrary random positions. Specifically, we randomly mask 15% to 40% of the tokens at the end of the sequence. Except for this, the other training strategy is exactly the same as the pre-training.

2) *CSI Classification Task*: For the CSI classification task, we adopt the approach commonly used for pre-trained models, where we freeze the bottom layers of CSI-BERT2 and only train the top layers for specific classification tasks. Different from CSI-BERT1, in this phase, we use [MASK] tokens to replace not only all [PAD] tokens but also some other input tokens randomly, to imitate the situation of different packet loss rates. By this way, our model has better generalization capacity, not limited to the scenarios in the training set.

F. Inferring Phase

1) *CSI Prediction Task*: In the inferring phase of the prediction task, we first use [MASK] to replace all [PAD] tokens, and then we fix the last 20% of tokens in the input

TABLE I
MODEL CONFIGURATIONS: THIS TABLE PROVIDES A DETAILED OVERVIEW OF OUR CSI-BERT2 IN THE FOLLOWING EXPERIMENTS. IN THIS CONTEXT, ‘M’ REPRESENTS ‘MILLION’ AND ‘K’ REPRESENTS ‘KILO’, WHICH WILL REMAIN CONSISTENT IN THE SUBSEQUENT TABLES.

Configuration	Our Setting
Input Length	100
Input Dimension	52
Network Layers	6
Hidden Size	128
Inner Linear Size	512
Attn. Heads	8
Dropout Rate	0.1
Optimizer	AdamW
Learning Rate	0.0005
Batch Size	64
Total Number of Parameters	5.45M

sequences as [MASK]. The model is then used to predict the last 20% of tokens.

2) *CSI Classification Task*: In the inferring phase of the classification task, there is no need to add extra [MASK] tokens as in fine-tuning, but only to use [MASK] to replace [PAD]. Furthermore, with the help of our time embedding, we find that our CSI-BERT2 model is able to effectively process data with different sampling rates, whereas traditional neural networks cannot always do this. For example, our model can successfully work when the testing data has a different sampling rate from the training data. The detailed experimental results will be shown in Section IV-C3.

IV. EXPERIMENT

A. Experiment Configuration

We illustrate our model configurations in Table I. We trained our model on an NVIDIA RTX 3090. During training, we observed that CSI-BERT occupied approximately 2500MB of GPU memory.

B. Dataset Description

In our experiment, we utilize three datasets: the publicly available WiGesture dataset [24], the WiFall Dataset [26], and a novel dataset named WiCount, which is proposed along with this paper. All these datasets are collected using the ESP32-S3 device as RX and a home router as TX, and share the same data format, with a sample rate of 100Hz, 1 antenna, and 52 subcarriers. For our experiment, we divide the data into 1-second samples, resulting in each sample having a length of 100 data points. We take the first 90% of the samples as the training set and the last 10% as the testing set within each category.

1) *WiGesture Dataset*: The WiGesture dataset is a gesture recognition and people identification dataset, containing the CSI collected from 8 individuals performing 6 different gesture actions, including left-right, forward-backward, and up-down motions, clockwise circling, clapping, and waving.

2) *WiFall Dataset*: The WiFall dataset is an action recognition, fall detection, and people identification dataset, containing the CSI collected from 10 individuals performing 5 different actions, including walking, jumping, sitting, standing

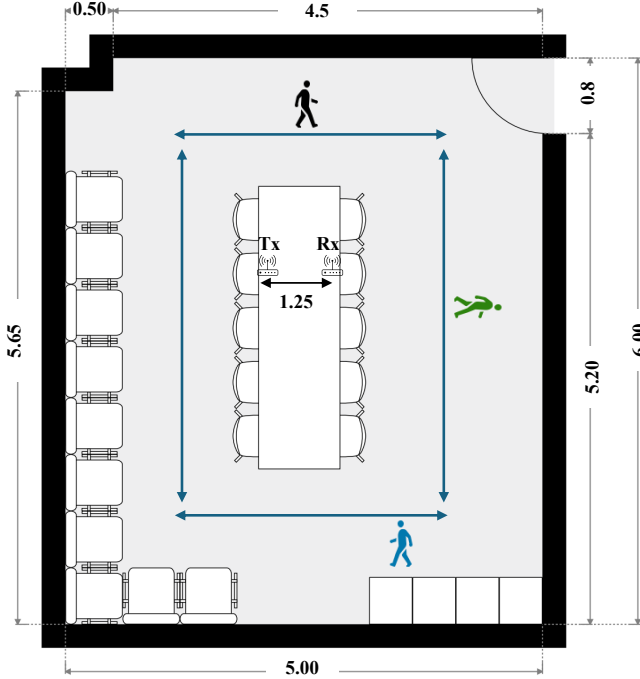


Fig. 5. Data Collection Environment of WiCount Dataset: The unit in the picture is meters.

up, and falling, which also consists of many types like forward fall, left fall, right fall, seated fall, and backward fall.

3) *WiCount Dataset*: The WiCount dataset is a people number estimation dataset, collected in a small meeting room as shown in Fig. 5. The sketch map of the dataset is illustrated as Fig. 6 that includes people number from 0 to 3. When collecting the data, people in the environment moved casually that they may jump, squat down, walk forward or backward, sit, and so on.

C. Experiment Result

1) *Pre-training Result*: In this section, we first illustrate the performance of our model during the pre-training phase, as this directly influences the model’s performance and convergence speed in downstream tasks. Following the approach taken by most signal generation studies [44], we evaluate pre-training performance using two metrics.

The first dimension is the signal recovery error. To demonstrate that CSI-BERT2 effectively learns the CSI pattern, we compare the recovery performance of our method against that of CSI-BERT1 and various traditional interpolation methods. Specifically, we assess the recovery performance by randomly deleting 15% of the packets and comparing the model’s recovery results with the ground truth. We employ Mean Squared Error (MSE), Symmetric Mean Absolute Percentage Error (SMAPE), and Mean Absolute Percentage Error (MAPE) to

quantify the error, as represented in Eq. 12:

$$\begin{aligned} \text{MSE}(\hat{c}_i, c_i) &= \frac{1}{n} \sum_{i=1}^n (c_i - \hat{c}_i)^2, \\ \text{SMAPE}(\hat{c}_i, c_i) &= \frac{1}{n} \sum_{i=1}^n \frac{|c_i - \hat{c}_i|}{\left(\frac{|c_i| + |\hat{c}_i|}{2} + \epsilon\right)}, \\ \text{MAPE}(\hat{c}_i, c_i) &= \frac{1}{n} \sum_{i=1}^n \frac{|c_i - \hat{c}_i|}{c_i + \epsilon}, \end{aligned} \quad (12)$$

where c_i and \hat{c}_i represent ground truth and model output respectively, n represents the number of samples, ϵ is a small number used to avoid division by zero. The metrics are calculated only on the 15% of the deleted CSI. Furthermore, to ensure fairness, we compute the error solely on the testing set, rather than on the entire dataset as done in CSI-BERT1. We also compare the time required to recover the full dataset across different models, using only the CPU for this comparison. Our results indicate that CSI-BERT2 achieves relatively low recovery error and recovery time across most datasets.

However, a low recovery error does not necessarily imply that the model has effectively learned the CSI pattern. For instance, the vanilla BERT model [20] also achieves a relatively low recovery error by producing similar outputs regardless of the input. Consequently, we adopt a common approach in generation studies by using the recovered data to train other models. If these models perform well on the generated data, it suggests that the recovered data is likely to be close to reality. Following the methodology of CSI-BERT1 [24], we provide two methods for CSI recovery, named “recover” and “replace”:

$$\begin{aligned} \text{CSI}^{\text{replace}} &= \hat{c}, \\ \text{CSI}^{\text{recover}} &= (1 - \text{IsPad}) \cdot c + \text{IsPad} \cdot \hat{c}, \\ \text{IsPad} &= (c == [\text{PAD}]), \end{aligned} \quad (13)$$

where *IsPad* indicates whether the position of the original CSI c corresponds to the [PAD] token.

Subsequently, we utilized the data recovered by the different methods to train various networks and evaluate their accuracy across multiple tasks, including gesture recognition, person identification, action recognition, fall detection, and crowd estimation. The models compared include traditional neural networks such as MLP, recently proposed architectures like LSTM [45], and Wi-Fi sensing models such as WiGRUNT [46]. The results are summarized in Table III. The findings clearly indicate that using CSI-BERT2 for data recovery yields the most significant improvements compared to other methods, suggesting that the data recovered by CSI-BERT2 is the closest to reality. Through these two aspects, we demonstrate the effectiveness of our pre-training method.

2) *CSI Prediction Task*: Due to the scarcity of real CSI data in wireless communication, we follow the approach taken by most previous studies and utilize wireless sensing datasets to evaluate model performance. For the prediction task, we provide the first 0.8 seconds of CSI in each sample and train the model to predict the subsequent 0.2 seconds of CSI. We compare the performance of our CSI-BERT2 model against several other CSI prediction models, including popular time series models like LSTM [45], RNN [47], GRU

TABLE II
RECOVERY ERROR: THE BOLD VALUE INDICATES THE BEST RESULT. THE ‘TIME(S)’ REPRESENTS THE DURATION THE MODELS TAKE TO INFER THE ENTIRE TESTING SET. THIS TERMINOLOGY WILL REMAIN CONSISTENT ACROSS SUBSEQUENT TABLES.

Dataset \ Metric Method	WiGesture [24]				WiFall [26]				WiCount			
	MSE	SMAPE	MAPE	Time(s)	MSE	SMAPE	MAPE	Time(s)	MSE	SMAPE	MAPE	Time(s)
CSI-BERT2	2.0800	0.1153	0.1217	5.53	4.1463	0.1240	0.1351	2.77	2.4531	0.1092	0.1189	1.56
CSI-BERT1 [24]	2.2438	0.1156	0.1244	1.84	4.4042	0.1271	0.1373	1.32	2.4471	0.1092	0.1185	0.67
Linear Interpolation	2.8642	0.1266	0.1364	38.49	6.4420	0.1461	0.1571	2.81	2.6870	0.1099	0.1175	1.20
Ordinary Kringing	3.5090	0.1390	0.1612	2709.43	4.6637	0.1319	0.1462	289.09	4.5964	0.1423	0.1684	109.10
Inverse Distance Weighted (IDW)	2.4726	0.1187	0.1301	19.82	4.4251	0.1276	0.1409	2.45	3.4431	0.1268	0.1483	0.82

TABLE III
CSI CLASSIFICATION PERFORMANCE: THE NUMBER BELOW EACH MODEL NAME REPRESENTS THE NUMBER OF PARAMETERS. THE BOLD VALUE INDICATES THE BEST RESULT IN EACH COLUMN, AND THE UNDERLINED VALUE INDICATES THE BEST RESULT IN EACH ROW WITHIN EACH TASK.

Task		Gesture Recognition (WiGesture Dataset [24])								
Model	MLP	CNN	RNN [47]	LSTM [45]	Chen et al. [48]	WiGRUNT [46]	CSI-BERT1 [24]	CSI-BERT2	Average	
Data	337K	23K	33K	133K	11M	11M	2M	5M		
Original Data	66.93%	55.72%	39.56%	11.97%	70.31%	48.73%	76.91%	99.48%	58.70%	
CSI-BERT2 recover	72.88%	57.27%	54.34%	48.35%	92.96%	78.97%	92.18%	89.06%	73.25%	
CSI-BERT2 replace	73.68%	62.80%	55.48%	40.79%	91.92%	74.99%	81.51%	91.95%	71.63%	
CSI-BERT1 recover	74.23%	59.39%	48.96%	22.92%	92.57%	71.87%	71.87%	92.70%	66.81%	
CSI-BERT1 replace	86.90%	61.51%	58.80%	52.36%	84.52%	78.84%	79.54%	91.41%	74.24%	
Linear Interpolation	72.91%	58.35%	45.32%	49.09%	80.75%	74.91%	74.55%	88.25%	68.01%	
Ordinary Kringing	65.62%	57.55%	53.64%	50.00%	88.71%	69.99%	74.27%	85.93%	68.21%	
IDW	40.17%	56.77%	48.70%	46.88%	80.32%	71.06%	67.22%	<u>88.28%</u>	62.42%	

Task		People Identification (WiGesture Dataset [24])								
Model	MLP	CNN	RNN [47]	LSTM [45]	Chen et al. [48]	WiGRUNT [46]	CSI-BERT1 [24]	CSI-BERT2	Average	
Original Data	71.34%	71.14%	66.39%	21.09%	83.76%	72.07%	93.94%	99.73%	72.43%	
CSI-BERT2 recover	95.57%	85.54%	84.60%	27.98%	93.20%	81.73%	97.92%	99.73%	83.28%	
CSI-BERT2 replace	95.05%	83.07%	84.68%	54.13%	95.33%	83.84%	96.35%	94.79%	85.91%	
CSI-BERT1 recover	97.13%	80.60%	80.51%	35.18%	94.30%	84.67%	95.05%	99.73%	83.39%	
CSI-BERT1 replace	97.65%	79.18%	89.24%	24.22%	97.39%	77.77%	95.83%	99.47%	82.59%	
Linear Interpolation	81.84%	70.88%	84.45%	26.83%	86.75%	70.28%	97.92%	91.67%	76.33%	
Ordinary Kringing	94.76%	85.38%	86.42%	21.61%	97.32%	80.84%	95.83%	99.03%	82.64%	
IDW	83.22%	74.56%	88.54%	33.91%	94.27%	80.70%	95.20%	99.47%	81.23%	

Task		Action Recognition (WiFall Dataset [26])								
Model	MLP	CNN	RNN [47]	LSTM [45]	Chen et al. [48]	WiGRUNT [46]	CSI-BERT1 [24]	CSI-BERT2	Average	
Original Data	47.48%	56.27%	58.61%	52.10%	51.38%	34.44%	82.43%	88.59%	58.91%	
CSI-BERT2 recover	64.97%	67.18%	68.48%	62.63%	71.70%	70.96%	67.63%	72.16%	68.21%	
CSI-BERT2 replace	69.01%	66.27%	70.18%	61.99%	73.96%	69.72%	66.77%	72.70%	68.82%	
CSI-BERT1 recover	66.40%	54.94%	68.48%	61.79%	69.66%	70.94%	67.36%	73.69%	66.65%	
CSI-BERT1 replace	73.05%	54.97%	66.79%	66.73%	72.01%	67.44%	66.61%	<u>73.67%</u>	67.65%	
Linear Interpolation	67.44%	64.32%	67.31%	59.78%	74.22%	70.57%	64.37%	74.19%	67.77%	
Ordinary Kringing	67.96%	65.52%	64.44%	63.88%	70.92%	62.41%	67.36%	<u>71.77%</u>	66.78%	
IDW	70.31%	67.08%	69.79%	62.32%	71.09%	72.39%	67.22%	70.21%	68.80%	

Task		Fall Detection (WiFall Dataset [26])								
Model	MLP	CNN	RNN [47]	LSTM [45]	Chen et al. [48]	WiGRUNT [46]	CSI-BERT1 [24]	CSI-BERT2	Average	
Original Data	78.34%	52.99%	82.29%	80.35%	78.52%	73.69%	93.28%	94.79%	79.28%	
CSI-BERT2 recover	80.79%	75.95%	86.58%	86.72%	82.42%	80.90%	82.25%	86.97%	82.82%	
CSI-BERT2 replace	79.82%	74.89%	83.07%	<u>86.31%</u>	82.16%	78.65%	80.62%	85.38%	81.36%	
CSI-BERT1 recover	80.98%	75.27%	84.37%	80.41%	81.38%	83.07%	81.32%	84.92%	81.46%	
CSI-BERT1 replace	80.21%	74.94%	83.46%	84.37%	82.33%	80.79%	83.33%	85.72%	81.89%	
Linear Interpolation	81.78%	75.78%	84.50%	84.33%	78.51%	78.77%	81.35%	84.39%	81.17%	
Ordinary Kringing	81.64%	75.78%	80.98%	82.29%	82.00%	79.03%	82.31%	84.49%	81.07%	
IDW	82.55%	54.94%	83.59%	80.59%	78.21%	80.72%	81.72%	84.06%	78.29%	

Task		People Number Estimation (WiCount Dataset)								
Model	MLP	CNN	RNN [47]	LSTM [45]	Chen et al. [48]	WiGRUNT [46]	CSI-BERT1 [24]	CSI-BERT2	Average	
Original Data	56.77%	69.68%	80.93%	80.72%	48.33%	49.53%	89.67%	94.32%	71.24%	
CSI-BERT2 recover	87.29%	78.75%	83.98%	81.51%	83.32%	85.42%	84.06%	91.32%	84.45%	
CSI-BERT2 replace	85.62%	78.49%	88.12%	86.97%	81.41%	82.34%	81.51%	92.76%	84.65%	
CSI-BERT1 recover	88.98%	80.83%	86.20%	82.39%	82.22%	82.70%	79.04%	92.70%	84.38%	
CSI-BERT1 replace	81.61%	72.60%	85.67%	84.95%	85.62%	82.75%	81.61%	92.86%	83.46%	
Linear Interpolation	76.51%	77.73%	85.52%	82.40%	80.17%	83.07%	86.51%	88.64%	82.57%	
Ordinary Kringing	87.29%	50.52%	84.84%	85.05%	82.97%	76.72%	85.72%	91.90%	80.63%	
IDW	80.72%	82.29%	84.17%	87.00%	82.10%	81.72%	85.62%	88.54%	84.02%	

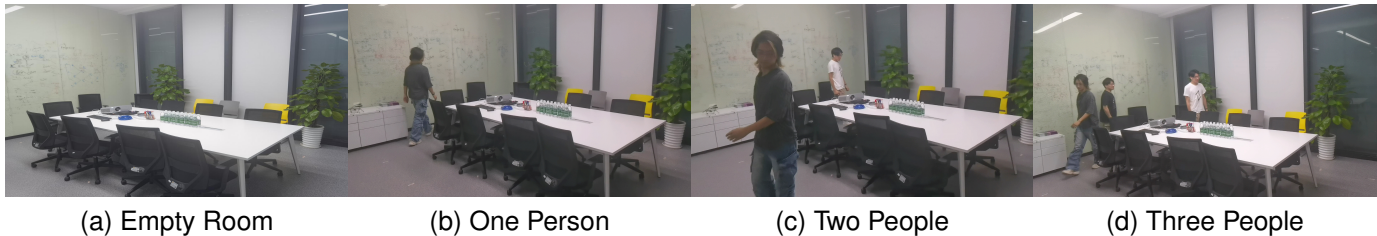


Fig. 6. Sketch Map of WiCount Dataset

TABLE IV
CSI PREDICTION ERROR

Dataset \ Metric	WiGesture [24]				WiFall [26]				WiCount			
	MSE	SMAPE	MAPE	Time(s)	MSE	SMAPE	MAPE	Time(s)	MSE	SMAPE	MAPE	Time(s)
CSI-BERT2 (5M)	3.2942	0.1583	0.1349	0.46	4.8598	0.1471	0.1347	0.49	5.3401	0.1726	0.1590	0.46
LSTM (133K) [45], [51]–[54]	12.3254	0.2397	0.3967	0.05	7.1495	0.1624	0.1882	0.04	32.3377	0.2547	0.3528	0.05
RNN (33K) [47], [55]	19.4708	0.2877	0.4063	0.04	16.9083	0.2424	0.2988	0.04	32.3670	0.2548	0.3534	0.03
GRU (100K) [49], [56]	19.7180	0.2922	0.4243	0.04	16.5353	0.2395	0.2963	0.07	39.8108	0.2541	0.3556	0.02
Mamba (5M) [50]	12.3281	0.2392	0.3277	0.24	6.4666	0.1532	0.1756	0.12	39.9170	0.2566	0.3524	0.11
OCEAN (126K) [57]	19.6257	0.2925	0.4231	0.05	16.8825	0.2423	0.2978	0.03	39.7917	0.2542	0.3548	0.02
CV-3DCNN (19K) [58]	11.3017	0.2267	0.3044	0.04	8.2616	0.1713	0.1981	0.03	42.2662	0.2631	0.3560	0.02
ConvLSTM (152K) [59]	19.7038	0.2921	0.4242	0.04	16.8935	0.2429	0.2983	0.03	39.7709	0.2537	0.3552	0.02

[49], and Mamba [50], which are also widely used in CSI prediction [51]–[56]. We also compare our model with some CSI prediction networks like OCEAN [57], CV-3DCNN [58], and ConvLSTM [59]. The prediction error and time cost (using GPU) are shown in Table IV. It can be seen that our CSI-BERT2 model significantly outperforms all other models. Particularly in the WiCount dataset, where the task is more challenging, as each gesture or action has a relatively irregular pattern, other methods exhibit a substantial decrease in performance, while CSI-BERT2 is influenced only minimally. Although the inference time of CSI-BERT2 is longer than that of the other models, its prediction time for the entire testing set across different datasets remains under 0.5 seconds, which is acceptable.

3) *CSI Classification Task*: The robust and powerful capabilities of our CSI-BERT2 model in CSI classification tasks are demonstrated in Table III, where it achieves the best performance across all scenarios. Moreover, with the aid of time embedding, our CSI-BERT2 can be employed in scenarios where the training set has samples with different sampling rates, or the testing set has a different sampling rate from the training set. This is a practical feature, especially in federated learning scenarios, where we cannot guarantee that all clients have the same sampling rate. In Table V, we compare the performance of different models where the training and testing sets both have 100Hz and 50Hz CSI, as well as where the training set only has 100Hz CSI but the testing set has 50Hz CSI. For fairness, we provide the CSI processed by linear interpolation for the other non-CSI-BERT models. It can be seen that other models are significantly influenced by the different sampling rates, with some even failing in particular scenarios. In contrast, CSI-BERT2 is almost unaffected by any impact, thanks to the help of its time embedding.

What’s more, resampling methods could also be a potential way to address such scenarios. However, on one hand, the

resampling operation may introduce a relatively high time delay. On the other hand, these resampling methods were not designed specifically for CSI, which means they may not be able to capture the inherent relationships within the CSI as traditional interpolation methods. The resampling error could also potentially harm the model’s performance.

D. Ablation Study

1) *Effect of Pre-training*: To illustrate the help of our pre-training mechanism for downstream tasks, we compare the model’s performance with and without pre-training, as shown in Fig. 7 and Table VI. In the CSI classification task, the improvement from pre-training is modest but not particularly significant. However, in the CSI prediction task, pre-training proves to be highly beneficial, likely because the prediction task is more closely related to the mask recovery task.

2) *Effect of Change on Original BERT Model*: To demonstrate the effectiveness of the modifications we made to BERT [20], we first compare the recovery performance of the original BERT (where we simply use a linear layer as the embedding and output layer to support the CSI format) with our modified version, as shown in Fig. 8. We observe that the amplitude spectrum of the original BERT appears smooth across all subcarriers, indicating that it tends to map all tokens within each subcarrier to similar value. Although BERT can also achieve a relatively low MSE of 5.26 in WiGesture dataset, it fails to capture any valuable information.

Next, we compare the attention patterns of the proposed CSI-BERT models with the original BERT. As shown in Fig. 9, we illustrate the mean of attention patterns across all attention heads. The attention patterns of CSI-BERT1 and CSI-BERT2 consist of multiple diagonals from left to right, which is interpretable. This is because in a short time interval, CSI always changes in a particular regular pattern. Additionally, it is reasonable that their attention patterns are

TABLE V
CSI CLASSIFICATION PERFORMANCE UNDER DIFFERENT SAMPLING RATE

Data	Training Set: 100Hz+50Hz; Testing Set: 100Hz+50Hz							
Model	MLP	CNN	RNN [47]	LSTM [45]	Chen et al. [48]	WiGRUNT [46]	CSI-BERT1 [24]	CSI-BERT2
Gesture Recognition	16.51%	14.54%	15.13%	17.37%	16.59%	74.47%	64.61%	97.04%
People Identification	13.47%	15.52%	13.41%	13.47%	13.72%	81.25%	70.83%	99.54%
Action Recognition	70.97%	67.67%	70.02%	59.63%	75.18%	66.78%	78.18%	88.35%
Fall Detection	81.10%	75.80%	83.92%	84.83%	85.98%	80.72%	92.98%	93.64%
People Number Estimation	84.03%	46.82%	81.25%	82.00%	80.09%	76.13%	86.93%	92.54%

Data	Training Set: 100Hz; Testing Set: 50Hz							
Model	MLP	CNN	RNN [47]	LSTM [45]	Chen et al. [48]	WiGRUNT [46]	CSI-BERT1 [24]	CSI-BERT2
Gesture Recognition	69.79%	20.38%	36.25%	27.15%	74.89%	71.37%	79.96%	97.81%
People Identification	87.29%	11.85%	82.29%	22.32%	87.22%	85.24%	94.44%	99.38%
Action Recognition	68.97%	51.96%	68.07%	60.26%	76.56%	73.21%	84.56%	88.53%
Fall Detection	80.83%	76.13%	80.17%	84.38%	78.61%	77.08%	94.19%	94.32%
People Number Estimation	82.22%	77.03%	84.43%	42.22%	68.89%	71.11%	89.10%	94.77%

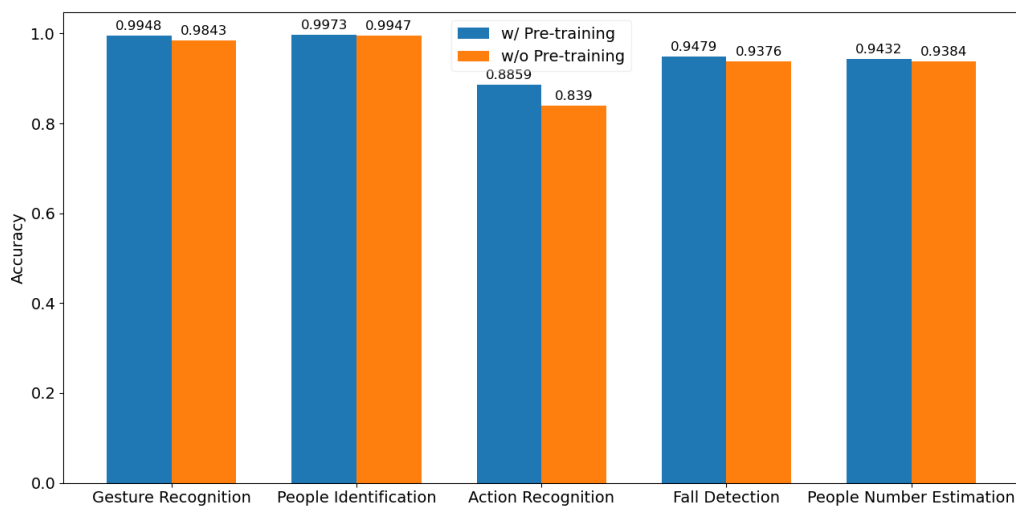


Fig. 7. CSI-BERT2 Performance in CSI Classification Task

TABLE VI
CSI-BERT2 PERFORMANCE IN CSI PREDICTION TASK

Dataset	w/ Pre-training			w/o Pre-training		
	MSE	SMAPE	MAPE	MSE	SMAPE	MAPE
WiGesture [24]	3.2942	0.1583	0.1349	5.3054	0.1962	0.1657
WiFall [26]	4.8598	0.1471	0.1347	5.0957	0.1595	0.1413
Wicount	5.4301	0.1726	0.1590	6.6868	0.2019	0.1659

approximately symmetric, which corresponds to the mechanism of bi-directional attention in BERT. However, we cannot find any regular patterns in the attention patterns of the original BERT.

Furthermore, we use a Gradient-weighted Class Activation Mapping (Grad-CAM) [60] method to provide explanations for the CSI recovery task of CSI-BERT and BERT. We manually delete a given package and use the models to recover them. After that, we calculate the Grad-CAM based on the gradient of the original input. We then combine it with the original input as shown in Fig. 10, which represents what the model mainly focuses on when recovering the deleted package. It can be seen that our CSI-BERT1 and CSI-BERT2 models mainly

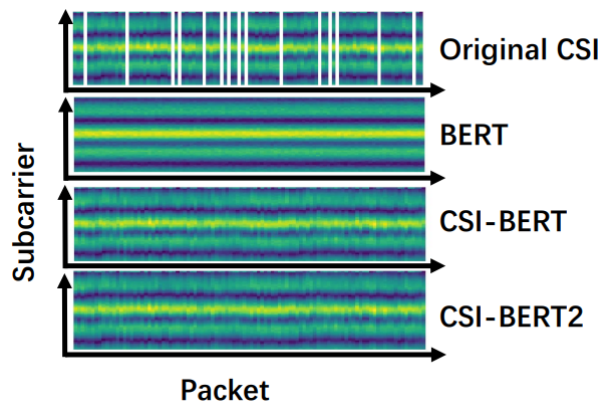


Fig. 8. Amplitude Spectrum of Original CSI and Output of BERT and CSI-BERT: The blank in the original CSI represents the lost CSI.

focus on packages nearby the lost package, which is consistent with our intuition. However, the original BERT only focuses on the lost package, which is actually meaningless because the

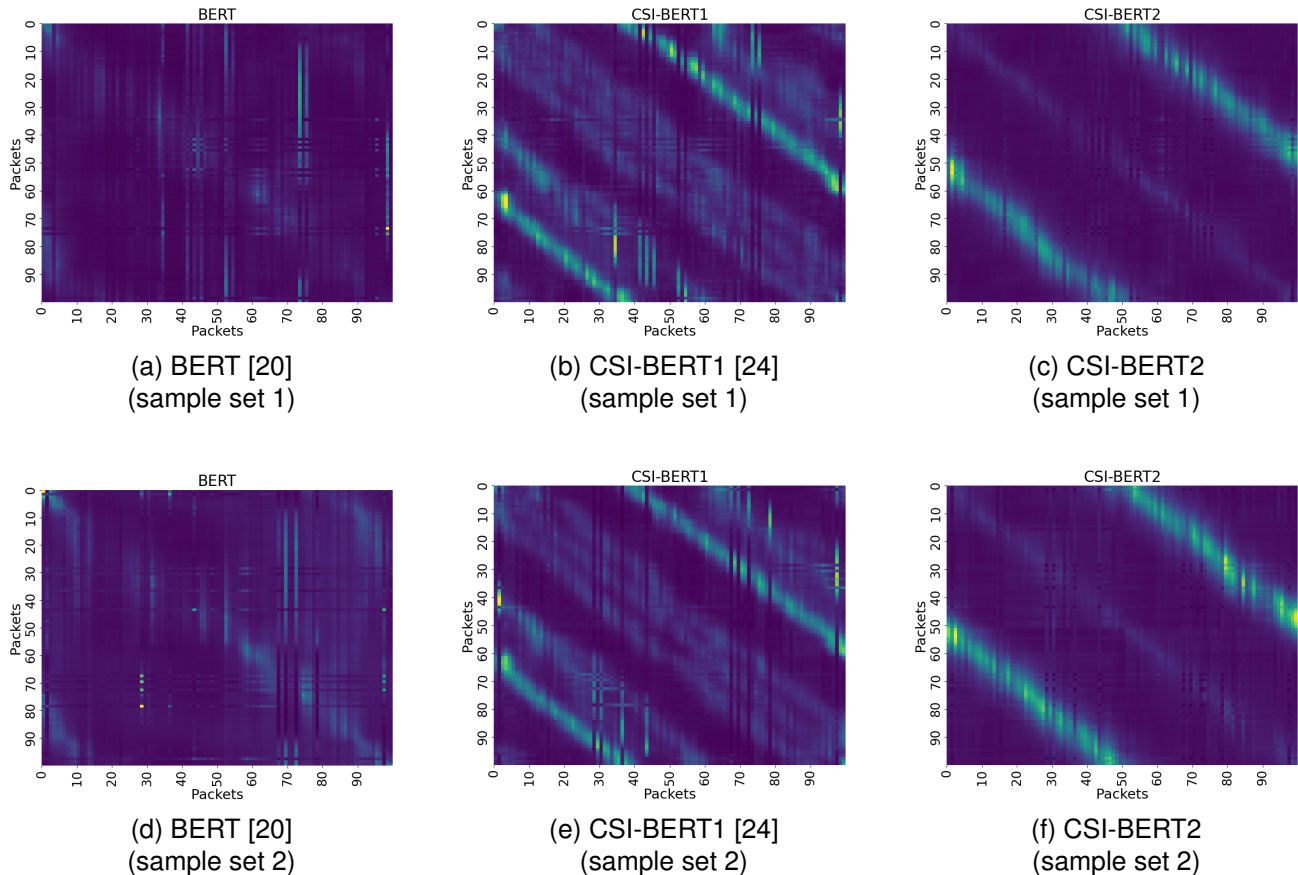


Fig. 9. Attention Patterns of Different Models: The heatmaps illustrate the mean attention patterns of three models. The two rows show the calculation results for two different sets of 100 CSI samples respectively. Here, lighter colors represent higher values, which remains consistent across subsequent figures.

lost package is replaced by [MASK] and can hardly provide useful information, except that the package at this position is lost.

V. CONCLUSION

In this paper, we introduce CSI-BERT2, a multifunctional model designed for CSI time series, encompassing CSI prediction, and classification. Through the proposed pre-training and fine-tuning methods, CSI-BERT2 effectively extracts valuable insights from limited CSI data. We have developed a novel time embedding mechanism to enhance the suitability of Transformer-based models for time series analysis. Additionally, we employed an ARL model to improve the model’s ability to capture relationships between different subcarriers. We also propose the MPM task, which fine-tunes BERT-based models specifically for prediction tasks. Furthermore, we have optimized the training process of CSI-BERT1, resulting in a significant enhancement in the model’s performance.

Through extensive experimentation, we demonstrate the effectiveness of CSI-BERT2. In the CSI prediction task, it significantly outperforms traditional models while maintaining relatively fast computation speeds. In the CSI classification task, it achieves state-of-the-art performance and can effectively handle scenarios where the training and testing sets contain samples with different sampling rates.

The CSI-BERT2 model can be further applied in other CSI-related scenarios and time-series tasks. Moreover, we aim to explore how to leverage multi-source heterogeneous CSI data to train our CSI-BERT simultaneously. By doing so, we hope to replicate the generalization capabilities of Large Language Models (LLMs) and Large Vision Models (LVMs) in the context of wireless sensing.

REFERENCES

- [1] G. Zhu, Z. Lyu, X. Jiao, P. Liu, M. Chen, J. Xu, S. Cui, and P. Zhang, “Pushing AI to wireless network edge: An overview on integrated sensing, communication, and computation towards 6G,” *Science China Information Sciences*, vol. 66, no. 3, p. 130301, 2023.
- [2] X. Li, F. Liu, Z. Zhou, G. Zhu, S. Wang, K. Huang, and Y. Gong, “Integrated sensing, communication, and computation over-the-air: MIMO beamforming design,” *IEEE Transactions on Wireless Communications*, 2023.
- [3] D. Wen, P. Liu, G. Zhu, Y. Shi, J. Xu, Y. C. Eldar, and S. Cui, “Task-oriented sensing, computation, and communication integration for multi-device edge AI,” *IEEE Transactions on Wireless Communications*, 2023.
- [4] Z. Cai, T. Chen, F. Zhou, Y. Cui, H. Li, X. Li, G. Zhu, and Q. Shi, “Falldewideo: Vision-aided wireless sensing dataset for fall detection with commodity wi-fi devices,” in *Proceedings of the 3rd ACM MobiCom Workshop on Integrated Sensing and Communications Systems*, pp. 7–12, 2023.
- [5] Z. Zhao, T. Chen, F. Meng, Z. Cai, H. Li, X. Li, and G. Zhu, “Lofi: Vision-aided label generator for wi-fi localization and tracking,” *arXiv preprint arXiv:2412.05074*, 2024.

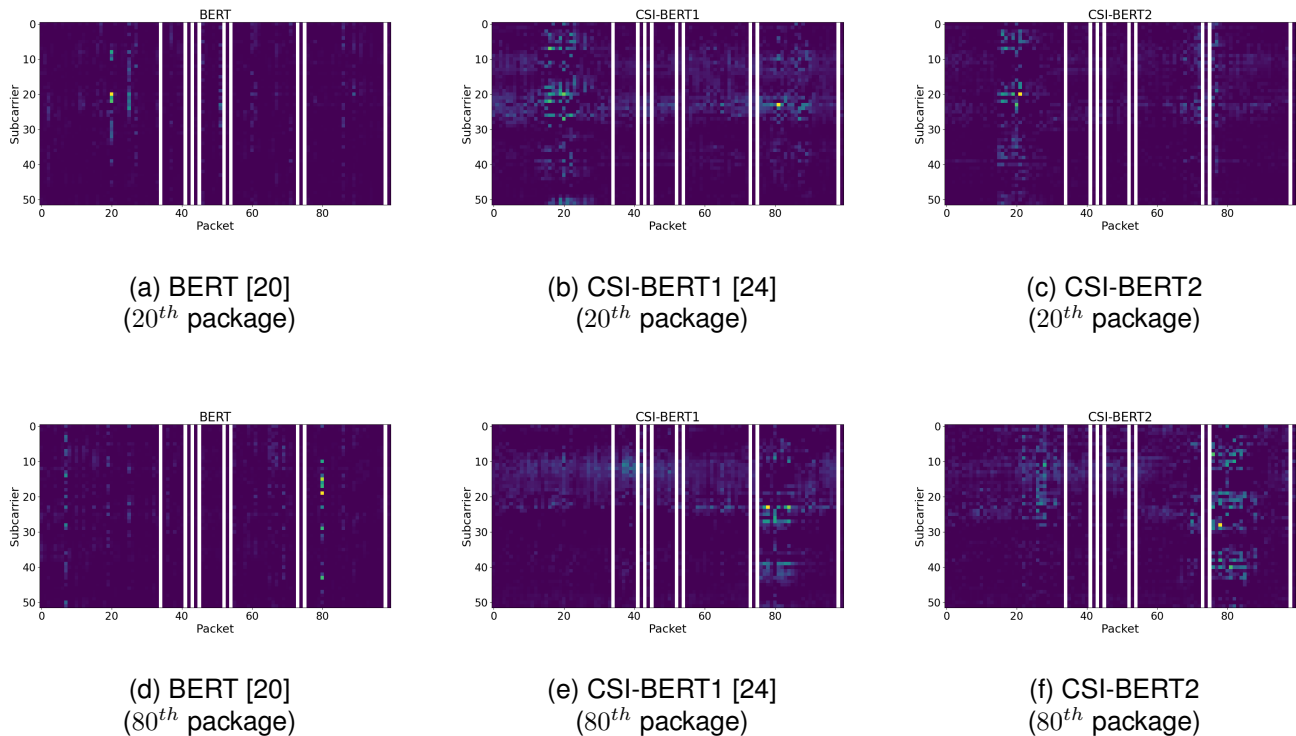


Fig. 10. Grad-CAM: The two rows of heatmaps illustrate the Grad-CAM when we manually delete a package at position 20 and position 80. The blank positions represent the actual lost CSI during transmission. We calculate Grad-CAM solely based on the loss function at the positions where we manually delete the packages.

- [6] Z. Zhao, T. Chen, Z. Cai, X. Li, H. Li, Q. Chen, and G. Zhu, "Crossfi: A cross domain wi-fi sensing framework based on siamese network," *arXiv preprint arXiv:2408.10919*, 2024.
- [7] M. Lewis, Y. Liu, N. Goyal, M. Ghazvininejad, A. Mohamed, O. Levy, V. Stoyanov, and L. Zettlemoyer, "Bart: Denoising sequence-to-sequence pre-training for natural language generation, translation, and comprehension," *arXiv preprint arXiv:1910.13461*, 2019.
- [8] A. Radford, K. Narasimhan, T. Salimans, I. Sutskever, *et al.*, "Improving language understanding by generative pre-training," 2018.
- [9] H. Bao, L. Dong, S. Piao, and F. Wei, "Beit: Bert pre-training of image transformers," *arXiv preprint arXiv:2106.08254*, 2021.
- [10] M. Germain, K. Gregor, I. Murray, and H. Larochelle, "Made: Masked autoencoder for distribution estimation," in *International conference on machine learning*, pp. 881–889, PMLR, 2015.
- [11] X. Liang, Z. Zhao, W. Zeng, Y. He, F. He, Y. Wang, and C. Gao, "Pianobart: Symbolic piano music generation and understanding with large-scale pre-training," *arXiv preprint arXiv:2407.03361*, 2024.
- [12] Z. Zhao, "Adversarial-midibert: Symbolic music understanding model based on unbiased pre-training and mask fine-tuning," *arXiv preprint arXiv:2407.08306*, 2024.
- [13] S. Wang, M. Khabza, and H. Ma, "To pretrain or not to pretrain: Examining the benefits of pretraining on resource rich tasks," *arXiv preprint arXiv:2006.08671*, 2020.
- [14] P. Ramachandran, P. J. Liu, and Q. V. Le, "Unsupervised pretraining for sequence to sequence learning," *arXiv preprint arXiv:1611.02683*, 2016.
- [15] T. Kojima, S. S. Gu, M. Reid, Y. Matsuo, and Y. Iwasawa, "Large language models are zero-shot reasoners," *Advances in neural information processing systems*, vol. 35, pp. 22199–22213, 2022.
- [16] S. Goyal, A. Kumar, S. Garg, Z. Kolter, and A. Raghunathan, "Finetune like you pretrain: Improved finetuning of zero-shot vision models," in *Proceedings of the IEEE/CVF Conference on Computer Vision and Pattern Recognition*, pp. 19338–19347, 2023.
- [17] S. J. Pan, "Transfer learning," *Learning*, vol. 21, pp. 1–2, 2020.
- [18] H. Chen, H. Chen, Z. Zhao, K. Han, G. Zhu, Y. Zhao, Y. Du, W. Xu, and Q. Shi, "An overview of domain-specific foundation model: key technologies, applications and challenges," *arXiv preprint arXiv:2409.04267*, 2024.
- [19] Y.-H. Chou, I.-C. Chen, J. Ching, C.-J. Chang, and Y.-H. Yang, "Midibert-piano: Large-scale pre-training for symbolic music classification tasks," *Journal of Creative Music Systems*, vol. 8, no. 1, 2024.
- [20] J. Devlin, M.-W. Chang, K. Lee, and K. Toutanova, "BERT: Pre-training of deep bidirectional Transformers for language understanding," *arXiv preprint arXiv:1810.04805*, 2018.
- [21] B. Guo, W. Zuo, S. Wang, W. Lyu, Z. Hong, Y. Ding, T. He, and D. Zhang, "WEPOS: Weak-supervised indoor positioning with unlabeled Wi-Fi for on-demand delivery," *Proceedings of the ACM on Interactive, Mobile, Wearable and Ubiquitous Technologies*, vol. 6, no. 2, pp. 1–25, 2022.
- [22] X. Sun, H. Ai, J. Tao, T. Hu, and Y. Cheng, "BERT-ADLOC: A secure crowdsourced indoor localization system based on BLE fingerprints," *Applied Soft Computing*, vol. 104, p. 107237, 2021.
- [23] Z. Wang, Q. Kong, B. Wei, L. Zhang, and A. Tian, "Radio map construction based on BERT for fingerprint-based indoor positioning system," *EURASIP Journal on Wireless Communications and Networking*, vol. 2023, no. 1, pp. 1–18, 2023.
- [24] Z. Zhao, T. Chen, F. Meng, H. Li, X. Li, and G. Zhu, "Finding the missing data: A bert-inspired approach against package loss in wireless sensing," *arXiv preprint arXiv:2403.12400*, 2024.
- [25] A. Zeng, M. Chen, L. Zhang, and Q. Xu, "Are transformers effective for time series forecasting?," in *Proceedings of the AAAI conference on artificial intelligence*, vol. 37, pp. 11121–11128, 2023.
- [26] Z. Zhao, Z. Cai, T. Chen, X. Li, H. Li, and G. Zhu, "Knn-mmd: Cross domain wi-fi sensing based on local distribution alignment," *arXiv preprint arXiv:2412.04783*, 2024.
- [27] Y. Ma, G. Zhou, and S. Wang, "Wifi sensing with channel state information: A survey," *ACM Computing Surveys (CSUR)*, vol. 52, no. 3, pp. 1–36, 2019.
- [28] C. Qi, P. Dong, W. Ma, H. Zhang, Z. Zhang, and G. Y. Li, "Acquisition of channel state information for mmwave massive mimo: Traditional and machine learning-based approaches," *Science China Information Sciences*, vol. 64, pp. 1–16, 2021.
- [29] Y. Yang, F. Gao, C. Xing, J. An, and A. Alkhateeb, "Deep multimodal learning: Merging sensory data for massive mimo channel prediction,"

- IEEE Journal on Selected Areas in Communications*, vol. 39, no. 7, pp. 1885–1898, 2021.
- [30] Y. Zhang, A. Alkhateeb, P. Madadi, J. Jeon, J. Cho, and C. Zhang, “Predicting future csi feedback for highly-mobile massive mimo systems,” *arXiv preprint arXiv:2202.02492*, 2022.
- [31] J. Yuan, H. Q. Ngo, and M. Matthaiou, “Machine learning-based channel estimation in massive mimo with channel aging,” in *2019 IEEE 20th International Workshop on Signal Processing Advances in Wireless Communications (SPAWC)*, pp. 1–5, 2019.
- [32] D. Wu, Y. Zeng, R. Gao, S. Li, Y. Li, R. C. Shah, H. Lu, and D. Zhang, “Witraj: Robust indoor motion tracking with wifi signals,” *IEEE Transactions on Mobile Computing*, vol. 22, no. 5, pp. 3062–3078, 2023.
- [33] D. Zhang, Z. Cai, G. Zhu, H. Li, X. Li, Q. Shi, and C. Shen, “Ratiofi: Unlocking the potential of wifi csi,” in *2023 International Conference on Ubiquitous Communication (Ucom)*, pp. 421–425, IEEE, 2023.
- [34] J. Yang, Y. Zhou, H. Huang, H. Zou, and L. Xie, “Metafi: Device-free pose estimation via commodity wifi for metaverse avatar simulation,” in *2022 IEEE 8th World Forum on Internet of Things (WF-IoT)*, pp. 1–6, 2022.
- [35] X. Zhu, T. Qiu, W. Qu, X. Zhou, M. Atiquzzaman, and D. O. Wu, “Bls-location: A wireless fingerprint localization algorithm based on broad learning,” *IEEE Transactions on Mobile Computing*, vol. 22, no. 1, pp. 115–128, 2023.
- [36] Y. Wang and J. Yang, “3d human mesh construction leveraging wi-fi,” *arXiv preprint arXiv:2210.10957*, 2022.
- [37] D. Wu, Y. Zeng, R. Gao, S. Li, Y. Li, R. C. Shah, H. Lu, and D. Zhang, “Witraj: Robust indoor motion tracking with wifi signals,” *IEEE Transactions on Mobile Computing*, vol. 22, no. 5, pp. 3062–3078, 2023.
- [38] A. Vaswani, N. Shazeer, N. Parmar, J. Uszkoreit, L. Jones, A. N. Gomez, Ł. Kaiser, and I. Polosukhin, “Attention is all you need,” *Advances in neural information processing systems*, vol. 30, 2017.
- [39] M. Sugiyama, M. Krauledat, and K.-R. Müller, “Covariate shift adaptation by importance weighted cross validation,” *Journal of Machine Learning Research*, vol. 8, no. 5, 2007.
- [40] T. Chen, Y. Wang, H. Chen, Z. Zhao, X. Li, N. Piovesan, G. Zhu, and Q. Shi, “Modelling the 5g energy consumption using real-world data: Energy fingerprint is all you need,” *arXiv preprint arXiv: 2406.16929*, 2024.
- [41] Y. Liu, M. Ott, N. Goyal, J. Du, M. Joshi, D. Chen, O. Levy, M. Lewis, L. Zettlemoyer, and V. Stoyanov, “RoBERTa: A robustly optimized BERT pretraining approach,” *arXiv preprint arXiv:1907.11692*, 2019.
- [42] Y. Ganin, E. Ustinova, H. Ajakan, P. Germain, H. Larochelle, F. Laviolette, M. March, and V. Lempitsky, “Domain-adversarial training of neural networks,” *Journal of machine learning research*, vol. 17, no. 59, pp. 1–35, 2016.
- [43] I. Goodfellow, J. Pouget-Abadie, M. Mirza, B. Xu, D. Warde-Farley, S. Ozair, A. Courville, and Y. Bengio, “Generative adversarial nets,” *Advances in neural information processing systems*, vol. 27, 2014.
- [44] H. He, H. Hu, X. Huan, H. Liu, J. An, and S. Mao, “Ai generated signal for wireless sensing,” in *GLOBECOM 2023-2023 IEEE Global Communications Conference*, pp. 6097–6102, IEEE, 2023.
- [45] S. Hochreiter and J. Schmidhuber, “Long short-term memory,” *Neural computation*, vol. 9, no. 8, pp. 1735–1780, 1997.
- [46] Y. Gu, X. Zhang, Y. Wang, M. Wang, H. Yan, Y. Ji, Z. Liu, J. Li, and M. Dong, “WiGRUNT: WiFi-enabled gesture recognition using dual-attention network,” *IEEE Transactions on Human-Machine Systems*, vol. 52, no. 4, pp. 736–746, 2022.
- [47] L. R. Medsker and L. Jain, “Recurrent neural networks,” *Design and Applications*, vol. 5, no. 64-67, p. 2, 2001.
- [48] T. Chen, X. Li, H. Li, and G. Zhu, “Deep learning-based fall detection using commodity wi-fi,” *Journal of Information and Intelligence*, 2024.
- [49] K. Cho, B. Van Merriënboer, C. Gulcehre, D. Bahdanau, F. Bougares, H. Schwenk, and Y. Bengio, “Learning phrase representations using rnn encoder-decoder for statistical machine translation,” *arXiv preprint arXiv:1406.1078*, 2014.
- [50] A. Gu and T. Dao, “Mamba: Linear-time sequence modeling with selective state spaces,” *arXiv preprint arXiv:2312.00752*, 2023.
- [51] T. Peng, R. Zhang, X. Cheng, and L. Yang, “Lstm-based channel prediction for secure massive mimo communications under imperfect csi,” in *ICC 2020-2020 IEEE International Conference on Communications (ICC)*, pp. 1–6, IEEE, 2020.
- [52] G.-Y. Chang, C.-K. Hung, and C.-H. Chen, “A csi prediction scheme for satellite-terrestrial networks,” *IEEE Internet of Things Journal*, 2022.
- [53] W. Jiang and H. D. Schotten, “Deep learning for fading channel prediction,” *IEEE Open Journal of the Communications Society*, vol. 1, pp. 320–332, 2020.
- [54] G. Liu, Y. Xu, Z. He, Y. Rao, J. Xia, and L. Fan, “Deep learning-based channel prediction for edge computing networks toward intelligent connected vehicles,” *IEEE Access*, vol. 7, pp. 114487–114495, 2019.
- [55] W. Jiang and H. D. Schotten, “Recurrent neural network-based frequency-domain channel prediction for wideband communications,” in *2019 IEEE 89th vehicular technology conference (VTC2019-Spring)*, pp. 1–6, IEEE, 2019.
- [56] A. Kulkarni, A. Seetharam, A. Ramesh, and J. D. Herath, “Deepchannel: Wireless channel quality prediction using deep learning,” *IEEE Transactions on Vehicular Technology*, vol. 69, no. 1, pp. 443–456, 2019.
- [57] C. Luo, J. Ji, Q. Wang, X. Chen, and P. Li, “Channel state information prediction for 5g wireless communications: A deep learning approach,” *IEEE transactions on network science and engineering*, vol. 7, no. 1, pp. 227–236, 2018.
- [58] Y. Zhang, J. Wang, J. Sun, B. Adebisi, H. Gacanin, G. Gui, and F. Adachi, “Cv-3dcnn: Complex-valued deep learning for csi prediction in fdd massive mimo systems,” *IEEE Wireless Communications Letters*, vol. 10, no. 2, pp. 266–270, 2020.
- [59] J. Wang, Y. Ding, S. Bian, Y. Peng, M. Liu, and G. Gui, “Ul-csi data driven deep learning for predicting dl-csi in cellular fdd systems,” *IEEE Access*, vol. 7, pp. 96105–96112, 2019.
- [60] R. R. Selvaraju, M. Cogswell, A. Das, R. Vedantam, D. Parikh, and D. Batra, “Grad-cam: Visual explanations from deep networks via gradient-based localization,” in *Proceedings of the IEEE international conference on computer vision*, pp. 618–626, 2017.